IEEE Access
Multidisciplinary | Rapid Review | Open Access Journal

Date of publication xxxx 00, 0000, date of current version xxxx 00, 0000.

*Digital Object Identifier 10.1109/ACCESS.2017.DOI*

# Evaluation of communication link performance and charging speed in self-powered Internet of underwater things devices

**BEHNAZ MAJLESEIN[1], (Student Member, IEEE), VICTOR GUERRA[2],JOSE RABADAN[3], ,JULIO RUFO[1,4], (Member, IEEE), and RAFAEL PEREZ-JIMENEZ.[3]**

[1]LightBee S.L., Las Palmas de Gran Canaria, Spain
[2]Pi Lighting Sarl, Sion, Switzerland
[3]IDeTIC, Universidad de Las Palmas de Gran Canaria, Las Palmas de Gran Canaria, Spain
[4]Ramon y Cajal Researcher, Universidad de La Laguna (ULL), 38208 San Cristobal de La Laguna

Corresponding author: Behnaz Majlesein (bmajlesein@lightbeecorp.com)

This work has been funded by the European Union's Horizon 2020 research and innovation programme under the Marie Skłodowska Curie grant agreement ENLIGHTEM No. 814215.

**ABSTRACT** The energy consumption of the Internet of underwater things (IoUT) nodes is a capital aspect that dramatically affects the applicability of wireless optical technologies in several scenarios, such as ocean monitoring or underwater sensor networks. Simultaneous lightwave information and power transfer (SLIPT) is a cost-effective and energy-efficient solution for energy-constrained wireless systems. Nonetheless, the reported battery-charging times for underwater operations are high, which should be improved to make this technology attractive enough to be considered for actual implementations. This paper provides a new SLIPT strategy, introducing a specific optical signal transmission scheme by controlling the transmitted direct current (DC) level component. The scheme is based on a DC-On Off Keying (OOK) modulation with an adjustable signal range (SR) to improve the energy-harvesting process and battery-charging time for underwater operations. The results reveal that the system provides a signal-to-noise ratio higher than 28 dB and the bit-error rate of less than $10^{-10}$ which is below the forward error correction limit with improved charging time around 30 minutes and 15 seconds for 5 F and 9.4 mF, respectively over 20 cm, and 63 seconds for 9.4 mF in 50 cm link distance.

**INDEX TERMS** Underwater wireless optical communications, energy harvesting, information decoding, simultaneous lightwave information and power transfer (SLIPT), Internet of underwater things (IoUT).

## I. INTRODUCTION

THE demand for underwater communication system links has increased due to the growing need for maritime applications, such as environmental monitoring, oil and gas field exploration, and surveillance [1]. The generally-deployed acoustic and radio frequency communication links are constrained by the low data rate and high attenuation in the aquatic environment, respectively [2], [3]. However, optical wireless communications have been shown to provide high bandwidth and low latency over moderate link distances [4], [5]. In addition, low deployment and operational costs, physical security, and commercially-available transceivers make this technology a promised approach for underwater wireless communications [6]. The main limiting factors of underwater wireless optical communication (UWOC) are the absorption and the scattering due to present particles in the seawater. These phenomena cause the loss of optical intensity and severe temporal pulse broadening, limiting both the link range and the maximum achievable data rate [7], [8]. Furthermore, power consumption is a critical aspect of underwater sensor networks due to the complexity and difficulty of replacing or recharging batteries. Therefore, a reliable energy-charging system is needed. Simultaneous lightwave information and power transfer (SLIPT) systems can simultaneously provide remote battery charging and data transmission by means of optical radiation [9].

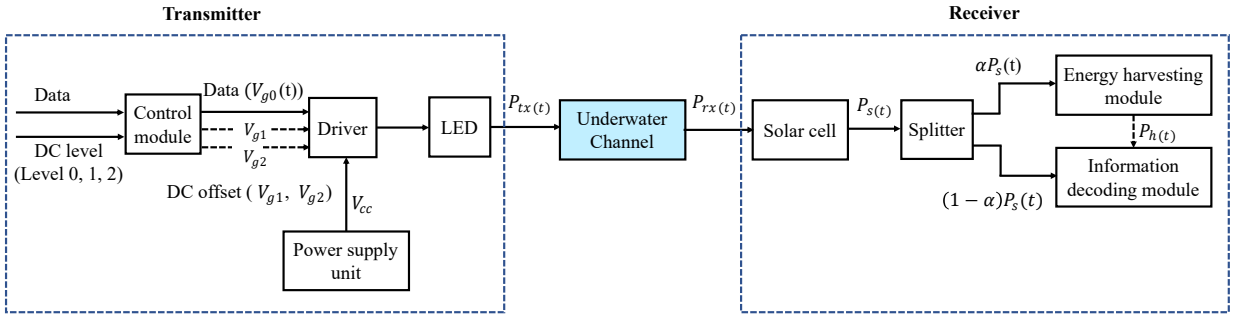


FIGURE 1: System block diagram.

There are three possible SLIPT approaches: time-splitting, power-splitting, and space-splitting. In a time-splitting approach, the receiver switches between energy harvesting (EH) and data decoding mode over different time slots. On the other hand, the power-splitting method is based on separating the received signal's power into alternating current (AC) and direct current (DC) components for information decoding (ID) and charging, respectively. Finally, in a space-splitting approach, multiple transmitters transfer either energy or information to the corresponding receivers for EH or ID [10], [11]. In the UWOC systems with SLIPT capability, a solar panel-based receiver for EH and ID is used [12]. In addition, although UWOC links are more robust to misalignment than atmospheric ones [13], the use of large detection areas improves their robustness. However, the low power conversion efficiency and slow response time of solar panels limit both the EH and communication performance of SLIPT systems, respectively [12]. In [14], a solar cell as a receiver without a lens and a 405 nm laser diode (LD) as a transmitter were used. The proposed system could transmit data over a 7 m link range, taking advantage of a large receiving area in a tap water channel under laboratory conditions. Moreover, spatial diversity reception can mitigate the deep fading that UWOC channels undergo under severe turbulent regimes [15]. In [16], Chen et al. proposed the use of a $2\times2$ solar panel array with a size of $10\times10$ mm$^2$ each as a receiver in an underwater laser-based link at 450 nm with a transmitted power of 19.76 dBm. The authors evaluated the system over a 7 m tap-water channel, achieving a data rate of 84 Mbps. The results showed that the system had a good performance in the presence of air bubbles and water fluctuation in terms of bit-error rate (BER) compared to using a single solar panel. In [17], amorphous silicon (a-Si) thin-film solar cell was used due to the higher light absorption coefficient in the visible light spectrum and lower cost than a crystalline-Si solar cell. A data rate of 908.2 Kb/s over a 2.4 m link range was achieved using a white-light laser. Kong et al. also essayed a white-laser-based link joint to two types of solar cells for two different purposes, a monocrystalline-Si solar cell for EH and an a-Si solar cell for ID. In addition, a hardware pre-equalizer to improve the 3-dB bandwidth was used. However, the mentioned system focused on communication performance, and the Si solar panel for EH was not connected to the system to operate underwater. The results showed the system was capable of achieving orthogonal frequency division multiplexing (OFDM) signals at the data rate of 1.2 Mbps over a transmission distance of 2 m under turbid water [18].

The studies mentioned above are mainly focused on communications performance. Therefore, solar panel performance in the case of EH needs to be investigated and optimized. In [19], the authors proposed a time-splitting SLIPT system using a 430 nm blue laser and $5.5\times7$ cm$^2$ solar cell to charge a battery with 840 mW of power capacity. The observed charging time of the battery was 124 minutes. Once fully charged, this hardware could activate a temperature sensor in a water tank for more than 2 hours. The sensor measured the temperature when the battery's voltage was higher than the threshold voltage of 3.6 V. Otherwise, it entered sleep mode to recharge the battery. Furthermore, a data rate of 500 Kb/s over a 1.5 m link range was achieved. In addition, De et al. used a 4.8 W LED as a transmitter for charging a 5 F capacitor to power an Internet of underwater things (IoUT) device, which took 90 minutes over a 30 cm link distance. Once the capacitor was fully charged, the device sent a real-time video streaming for 1 minute. Although the charging time for EH was considered in the mentioned work, no approach was proposed to decrease it. However, in [11] the optimization of the splitting factor (either in time or power) in terms of harvested energy while satisfying BER and spectral efficiency constraints was analyzed. In addition, closed-form equations were derived for the average harvested energy, BER, and spectral efficiency under the presence of underwater turbulence, which was modeled using a log-normal distribution. Uysal et al. improved the charging time by an optimization spilliting factor. However, to the best of the author's knowledge, the impact of the transmitted waveform on EH and communication performance in SLIPT UWOC systems has not been analyzed.

In this work, a new power-splitting SLIPT scheme is proposed to improve the energy harvesting rate for IoUT applications. The proposed system comprises a white-light LED (WLED) source and a solar cell as a receiver for both EH and ID. White-light laser sources are more favorable in increasing the energy conversion efficiency of the solar cells than red/blue-light lasers [14], [20]. However, LDs require

better alignment compared to LEDs, and their lifetime is limited. Furthermore, non-coherent light performs better in turbulent water [12], [21]. The main objective of this contribution is the reduction of the battery charging time, allowing the sensors to recharge and communicate in a reasonable time. The proposed transmitter scheme includes an adjustable signal range (SR) of the data or DC level component to trade-off between the higher signal-to-noise (SNR) and faster battery recharging depending on the channel condition. In this paper, SR refers to the difference between the maximum and minimum values of the signal over a period. To the best of the author's knowledge, this technique for improving the recharging time is mentioned for the first time in this paper. Furthermore, the reception stage circuitry includes a boost converter connected to the solar cell to step up the output voltage from its input and provide a stabilized supply voltage for the system.

The rest of this work is organized as follows. In section II, the system architecture is represented. Then, in Section III, the simulation and the experimental setups are described. Next, the results are explained and discussed in Section IV. Finally, the concluding remarks are provided in Section V.

## II. SYSTEM ARCHITECTURE

Figure 1 shows a block diagram of a power-splitting UWOC SLIPT system. A non-return-zero (NRZ) On-Off Keying (OOK) data signal is generated and is sent to a controller module which introduces different DC levels (.e.g., Level 0, Level 1, Level 2), which are provided by $V_{\mathrm{g1}}$ or $V_{\mathrm{g2}}$ with data signal of $V_{\mathrm{g0}}$ to the WLED's driver (the scheme and performance of the driver will be detailed in this paper). Moreover, a power supply is used to provide the DC bias ($V_{\mathrm{cc}}$) to supply the WLED transmitter. The modulated light beam ($P_{\mathrm{tx}}$) is transmitted through the underwater channel to the receiver, where the incoming optical light ($P_{\mathrm{rx}}$) is collected by the solar cell and converted to an electrical signal ($P_{\mathrm{s}}$). The received power is split into $\alpha\ P_{\mathrm{s}}$ and $(1 - \alpha)\ P_{\mathrm{s}}$ quantities for EH and ID by a splitter, respectively. The receiver can detect and decode the data signal when there is enough harvested energy ($P_{\mathrm{h}}$).

In this work, the performance of a UWOC system with SLIPT capability using the power splitting technique for both EH and ID is analyzed. Nevertheless, it mainly focuses on improving the energy harvesting rate, which determines the recharging time for the nodes to start working. In order to improve the energy harvesting time, a specific transmission scheme to adjust the SR or DC components of the transmitted optical signal is presented.

### A. TRANSMITTER

The main problem for EH in underwater environments is the long time needed to recharge the capacitor or the battery due to the high attenuation of the transmitted power and lack of enough ambient light. Therefore, improving the charging speed is essential for optimizing different system features, such as response time or data-logging periods. Once the capacitor is recharged to the threshold voltage, the harvested energy can be applied to supply IoUT nodes [22]. The recharging time depends on several factors, such as average transmitted power, link distance, solar cell size, power conversion efficiency, battery capacity, etc. In addition, the average transmitted power can be controlled by adjusting the signal DC level, affecting the energy harvesting performance. In this study, different discrete DC levels have been defined, and the best-performing ones can be selected depending on both the channel and device state conditions. The variation in the DC level component introduces changes in the SR of the AC (data signal) component since the higher the DC level, the lower the SR. Hence, a trade-off between EH and communication performances can be considered for selecting the appropriate DC level. Figure 2 shows the proposed transmission circuit scheme. In this circuit, three MOSFET transistors have been considered. $M_0$ controls an OOK modulated signal. Moreover, by switching on $M_1$ or $M_2$, the low level of the OOK signal rises. As a result, the DC level of the signal increases, thus increasing the average transmitted power. However, the SR of the AC signal decreases. A generalization of this scheme includes several MOSFETs to provide a range of discrete DC levels based on the value of resistors ($R_1$, $R_2$, ..., $R_{\mathrm{i}}$ , $\mathrm{i} \geq 1$) in the MOSFET drains. In this work, the proposed system provides four possible DC levels by setting the different MOSFET in ON-OFF states. As a general rule, $N$ transistors can provide $2^{\mathrm{N}-1}$ different DC levels. Therefore, depending on channel and device state conditions, the DC level can be adapted to increase harvested energy or SR. For instance, higher DC levels reduce the battery charging time. Conversely, lower DC levels provide higher SRs and improve SNRs. The output optical power is given by:

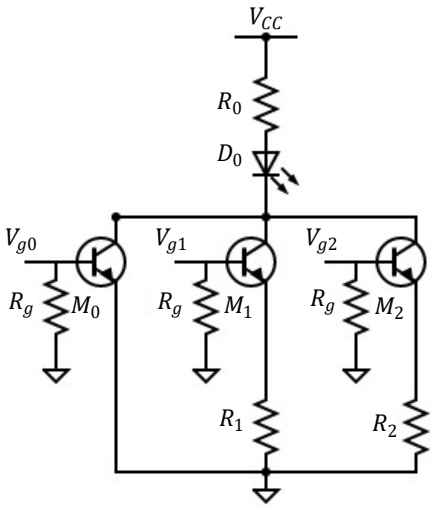


FIGURE 2: Proposed transmission scheme circuit.

$$P_{tx}(t) = P_{max} - SR \cdot s(t), \tag{1}$$

where $P_{\text{tx}}$ is the output optical power waveform, $P_{\max}$ is the maximum output power controlled by $R_0$ (shown in Fig. 2), and $s(t)$ is the transmission OOK waveform (i.e., 0 or 1).

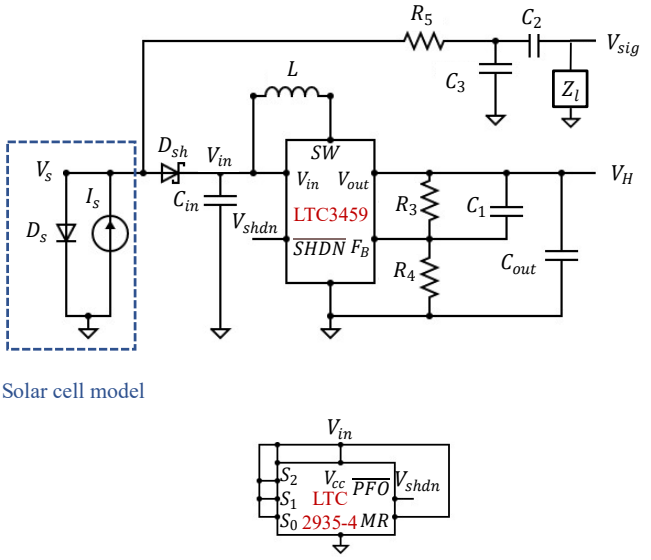


Solar cell model

FIGURE 3: Simulation setup of the proposed receiver circuit for simultaneous energy harvesting and communication.

### B. RECEIVER

As shown in Fig. 3, the obtained signal from the solar cell is divided into two branches for EH and ID, and the photo-generated current $I_{\text{s}}$ in an aquatic environment is governed by:

$$I_s(t) = \int_{\lambda} P_{opt}(t,\lambda) R(\theta,\varphi) \cdot e^{-c'(\lambda)d} \frac{A_{sc}}{d^2} \cos\Psi \mathrm{d}\lambda, \quad (2)$$

where $R(\theta,\varphi)$ is the radiation pattern of the optical source at elevation angle $\theta$ and azimuthal angle $\varphi$, $d$ is the link range, $c'(\lambda)$ is the extinction factor considering both absorption and multiple scattering [7], $\lambda$ is the wavelength of light, $\Psi$ is the impact angle, and $A_{\text{sc}}$ is the solar cell's active area.

As can be observed in Fig. 3, the SLIPT circuit presents the ID branch for the signal detection (upper branch) and the EH branch, which is isolated by the Schottky diode and the energy storage capacitor ($C_{in}$). In addition, The harvester circuit includes a DC-DC boost converter that starts working at the input voltage around 1.7 V and steps the output voltage up to 3.3 V. The boost converter increases the speed of supplying the required output voltage and maintains the power for a longer time. The photo-generated current of the solar cell is split into three branches as given by:

$$I_{\text{s}} = I_{\text{D}_{\text{s}}} + I_{\text{D}_{\text{sh}}} + I_{\text{F}}, \quad (3)$$

where $I_{\text{D}_{\text{s}}}$, $I_{\text{D}_{\text{sh}}}$ and $I_{\text{F}}$ are the current of diode $D_{\text{s}}$, the EH and ID branches current, respectively.

The current of each stage from Fig. 3 can be expressed as:

$$I_{\text{D}_{\text{s}}} = I_{\text{S}_0}\left(e^{\frac{V_{\text{s}}}{n_0 V_{\text{T}}}} - 1\right); V_{\text{T}} = \frac{KT}{q}, \quad (4)$$

$$I_{\text{D}_{\text{sh}}} = I_{\text{S}_1}\left(e^{\frac{V_{\text{D}_{\text{sh}}}}{n_1 V_{\text{T}}}} - 1\right), \quad (5)$$

and

$$I_{\text{F}} = \frac{V_{\text{s}}}{Z_{\text{F}}} \quad (6)$$

where $I_{s_{0,1}}$ is the reverse saturation current, $q$ is the elementary charge, $k$ is the Boltzmann constant, $T$ is the absolute temperature, $n_{0,1}$ is the diode ideality factor, $V_{\text{T}}$ is the thermal voltage, and $Z_{\text{F}}$ is the equivalent impedance of the ID stage, including the load impedance of the amplification front-end. $Z_{\text{F}}$ is obtained as:

$$Z_{\text{F}} = R_5 + \frac{1 + sC_2Z_{\text{l}}}{sC_2 + sC_3(1 + sC_2Z_{\text{l}})}. \quad (7)$$

In addition, $V_{\text{D}_{\text{s}}}$ and $V_{\text{D}_{\text{sh}}}$ are the voltage across the $D_{\text{s}}$ and $D_{\text{sh}}$, respectively as given by:

$$V_{\text{D}_{\text{sh}}} = V_{\text{s}} - V_{\text{in}}, \quad (8)$$

and the voltage across the capacitor is defined as:

$$V_{\text{in}}(t) = \frac{1}{C_{\text{in}}} \int I_{\text{D}_{\text{sh}}}(t)\, \mathrm{d}t. \quad (9)$$

By substituting 4, 5 and, 6 in 3, we have:

$$I_{\text{s}} = I_{\text{S}_0}\left(e^{\frac{V_{\text{s}}}{n_0 V_{\text{T}}}} - 1\right) + I_{\text{S}_1}\left(e^{\frac{V_{\text{s}} - V_{\text{in}}}{n_1 V_{\text{T}}}} - 1\right) + \frac{V_{\text{s}}}{Z_{\text{F}}}. \quad (10)$$

This equation is nonlinear. Therefore, to simplify the receiver circuit model, two stages can be considered. (i) At the beginning of the process, the LED starts the energy emission, and $C_{\text{in}}$ begins charging from the constant current provided by the solar cell ($I_{\text{D}_{\text{sh}}}$), and the rest of the circuit can be neglected. In this state, the equivalent impedance in the EH branch is less than in the data detection branch. Thus, the received signal passes to the EH branch more than the ID branch. Accordingly, the bandpass filter output ($V_{\text{sig}}$) is minimum. In this configuration, the diode $D_{\text{sh}}$ is in ON mode with a short circuit behavior ($Z_{\text{D}_{\text{sh}}} \approx 0$). This state is maintained until $V_{\text{in}}$ reaches the threshold voltage of the boost converter (in $t = t_{\text{s}}$), which enables it to supply the output voltage of 3.3 V. Then, the rest of the circuit begins operating and consuming the energy stored in the input capacitor through the boost converter. In the case that the transmitter can provide enough optical power to the system, the input capacitor can provide the necessary power to maintain the circuits working and continue charging. Following the diode I-V curve in Fig. 4, as $V_{\text{in}}$ increases, the diode voltage reduces, and its impedance increases. (ii) When $V_{\text{in}}$ reaches a voltage higher than ($V_{\text{s}} - V_{\text{D}_{\text{sh}}}$), the diode enters OFF mode, and the equivalent circuit consists of the bandpass filter only. Considering the voltage divider, $V_{\text{sig}}$ yields the following expression:

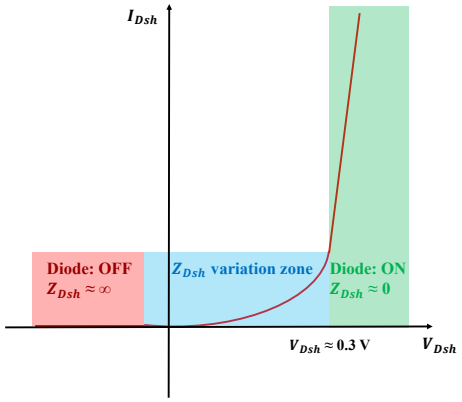


FIGURE 4: I-V diode curve.

$$\frac{V_{\text{sig}}}{V_{\text{s}}} = \frac{sC_2Z_{\text{L}}}{1 + s\left(C_2(Z_{\text{L}} + R_5) + C_3R_5\right) + s^2C_2C_3Z_{\text{L}}R_5}. \tag{11}$$

In this steady-state regime ($V_{\text{in}} = V_{\text{in(max)}}$), the AC signal is no longer affected by the input capacitor ($C_{\text{in}}$) and depends on the variation of $V_{\text{s}}$. Thus, the maximum detected SR in the ID branch ($V_{\text{sig(max)}}$) and the best SNR performance of the system are obtained. A general schematic of this behavior is shown in Fig. 5.

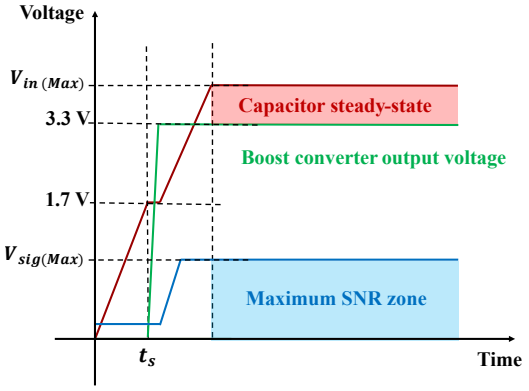


FIGURE 5: Receiver behavior scheme. Red, green, and blue curves correspond to the input capacitor voltage ($V_{\text{in}}$), the boost converter output voltage ($V_{\text{H}}$), and the voltage of the detected AC signal ($V_{\text{sig}}$), respectively.

On the other hand, the higher the boost converter's input capacitor, the higher the harvested energy and, therefore, the longer the charging time. Thus, the best input capacitor value can be selected depending on the required IoUT applications. The boost converter's shutdown (SHDN) pin is connected to the ultra-low-power supervisor with power-fail output and selectable thresholds to control the boost converter's switching. Hence, the boost converter stops working once the input capacitor's voltage falls below 1.7 V. The boost converter's current consumption is around 10 $\mu$A in an active mode. In addition, the solar cell in the proposed circuit scheme is used in a photovoltaic mode with less power consumption and easier integration in EH applications. However, it suffers from limited bandwidth. Furthermore, according to the solar cell I-V characteristic curve, the voltage variation becomes smaller as the current increases, with the possibility of saturating in environments including the presence of other light sources. However, the proposed system works perfectly in a deep, low-light marine environment.

TABLE 1: Simulation system parameters.

| Parameters | Value |
|---|---|
| $R_0$ | 100 Ω |
| $R_1$ | 56 Ω |
| $R_2$ | 6.8 Ω |
| $R_3$ | 1960 kΩ |
| $R_4$ | 1150 kΩ |
| $R_5$ | 39 Ω |
| $R_{\text{g}}$ | 1 kΩ |
| $C_1$ | 47 pF |
| $C_2$ | 4.7 $\mu$F |
| $C_3$ | 47 nF |
| $C_{\text{in}}$ | 9.4 mF, 5 F |
| $C_{\text{out}}$ | 100 $\mu$F |
| $V_{\text{cc}}$ | 14 V |
| $V_{\text{g0}}$ | 5 V, T=0.025 ms* |
| $V_{\text{g1}}$ | Variable 0 or 5 V |
| $V_{\text{g2}}$ | Variable 0 or 5 V |

*T is the signal period.

## III. METHODOLOGY

This section presents the performed analysis to validate the features of the proposed scheme described in the previous sections. The system is evaluated analytically through simulation and experimentally under a laboratory testbed condition, which will be described later in the paper. In section III-A, the system performance of the proposed transmission and reception schemes with their results are described, and in section III-B, the proposed solar cell-based UWOC system is experimentally evaluated in a water tank filled with tap water.

### A. SIMULATION STUDY ON TRANSMITTER AND RECEIVER SCHEMES

As mentioned, the transmitter stage is intended to control the average emitted power by adjusting the DC signal level. The transmission scheme presented in Fig. 2 is simulated in LTspice. In that scheme, $D_0$ represents the LED model, $M_0$ provides the data modulation control, $M_1$ and $M_2$ are DC level controllers, and $R_1$= 56 Ω and $R_2$= 6.8 Ω are selected based on the desired DC voltages or SRs. In the simulation, $Vg_0$, $Vg_1$, and $Vg_2$ are the gate's control voltages of $M_0$, $M_1$, and $M_2$, respectively. $Vg_0$ carries the modulated NRZ-OOK signal, $Vg_1$, and $Vg_2$ control signals for adjusting the different obtained voltage DC levels or SRs by switching $M_1$

or $M_2$ on or off, while $M_0$ is on. The LED current in different DC levels is illustrated in Fig. 6. In this work, the three most significant DC levels provided by the circuit of Fig. 2 are considered. Level 0 indicates when only $M_0$ is on, and Level 1 and Level 2 show the results when $M_1$ and $M_2$ are on, respectively, while $M_0$ remains switched on. On the receiver side, the solar cell in the simulation is modeled by a current source and six diodes, represented as $I_{\rm s}$ and $D_{\rm s}$ in Fig. 3, respectively. The input capacitor ($C_{\rm in}$) charges up to almost the voltage of $D_{\rm s}$, which corresponds to the solar cell's output voltage. As shown in Fig. 3, the received power is split into two branches for EH and ID. The detected SR, input, and output voltage of the boost converter are shown in Fig. 7. The $C_{\rm in}$ in the harvesting stage starts to charge. Once $V_{\rm in}$ reaches 1.7 V, the boost converter starts working and provides 3.3 V output voltage. As can be seen, the detected SR depends on the variations of the input capacitor voltage, and when the input capacitor is fully charged, the detected SR reaches its maximum amount. An LTC2935 component controls the SHDN pin, which switches the boost converter off when the input capacitor's voltage is below 1.7 V; otherwise, the boost converter is on.

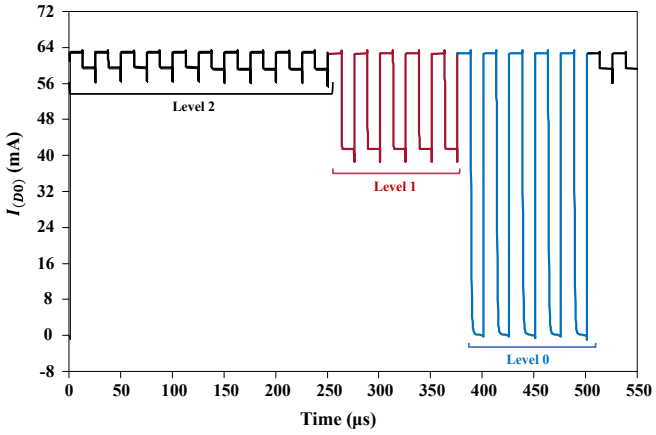


FIGURE 6: Simulation result of demonstrating the LED's current ($I_{\rm D0}$) in three different DC levels.

### B. EXPERIMENTAL SETUP

In this section, the experimental setup of the proposed UWOC SLIPT system based on power splitting configuration is described. Table 2 shows the system parameters used in the experiment. Figure 8 illustrates the general system block diagram and the experimental setup of the proposed solar cell-based UWOC system. A 10 W WLED is used as the transmitter derived from the circuit scheme shown in Fig. 2. The NRZ-OOK modulated signal is generated using an Arduino Uno microcontroller. As mentioned in the previous section, the proposed transmission scheme can control the low voltage level of the transmitted signal, thus, the total average transmitted power. In this work, based on the required DC levels (or SRs), $R_1$=56 Ω and $R_2$=6.8 Ω branches are selected. Then, $M_1$ or $M_2$ using the microcontroller are

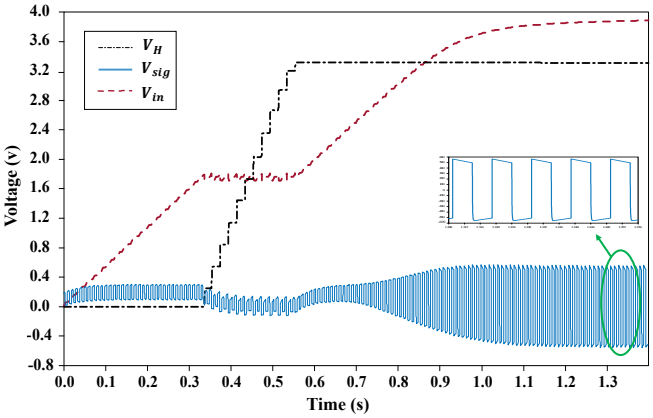


FIGURE 7: Simulation result illustrating the output voltage of the boost converter ($V_{\rm H}$), the received signal ($V_{\rm sig}$) and the charging curve of the input capacitor ($V_{\rm in}$).

TABLE 2: Experimental system parameters.

| Parameters | Value |
|---|---|
| LED light | White color |
| LED power | 10 W |
| Modulation | NRZ-OOK |
| Power supply characteristic | 14 V, 0.72 A |
| Tank dimension | 100×40×50 cm$^3$ |
| Link distance ($d$) | 20 cm, 50 cm |
| Water type | Tap water |
| Solar cell | Monocrystalline silicon |
| Solar cell dimension | 5×7 cm$^2$ |
| 3-dB bandwidth | 100 Hz |

switched on while $M_0$ is controlled by a 100 Hz NRZ-OOK modulation since it is limited by the 3-dB modulation bandwidth of the used solar cell. After transmitting through a water tank filled with tap water in 20 cm and 50 cm link distances, a light spot is formed on a 5× 7 cm$^2$ solar cell. The proposed system is based on the power splitting technique. Therefore, the received power is divided into two streams for detecting the signal and harvesting the energy as depicted in Fig. 3. The water tank side walls are covered by a black material to avoid reflections. The 3-dB system bandwidth is limited by the solar cell; however, it is sufficient for IoUT applications. In the experiment for detecting the AC signal, only a capacitor of 10 nF is used. The signal is captured and observed using the oscilloscope. The laptop is connected through an Ethernet connection to the oscilloscope to record the received signal. In practical applications, the receiver can detect and decode the data signal when there is enough harvested energy.

## IV. EXPERIMENTAL RESULTS

Figure 9 indicates the three different received voltage signals with the three DC levels; Level 0 represents when only $M_0$

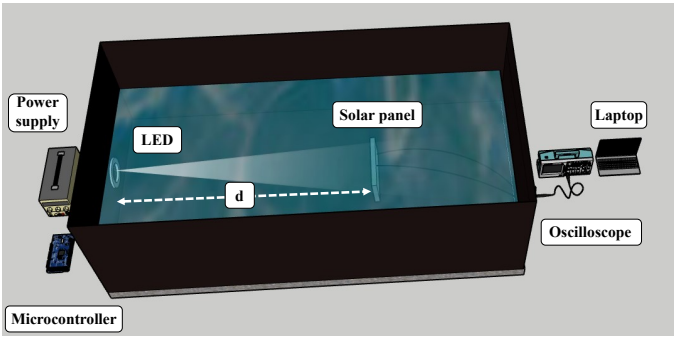


(a) Schematic illustration of the underwater SLIPT demonstration.

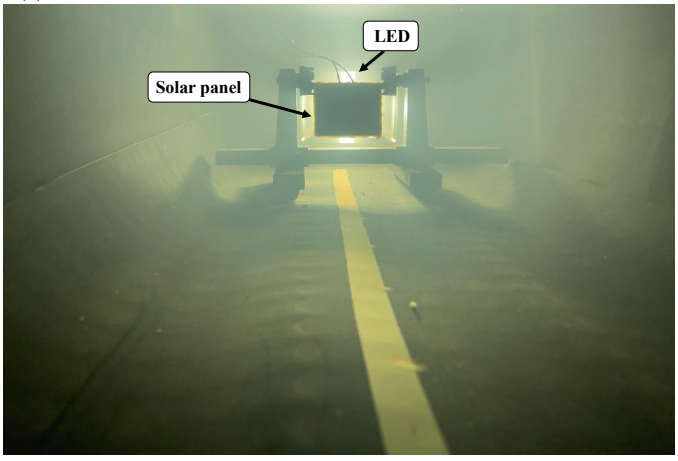


(b) Actual experimental setup of the proposed underwater SLIPT system.

FIGURE 8: Experimental setup of the underwater SLIPT system.

TABLE 3: Results obtained under the laboratory testbed condition in three different DC levels.

| **Levels** | **LED illuminance (klux)** | $t_{\mathrm{fc}}$ **5F (h)** | $t_{\mathrm{fc}}$ **9.4 mF (s)** | $I_{\mathrm{out}}$ **(mA)** | **d (cm)** |
|---|---|---|---|---|---|
| 0 | 3.05 | 3.6 | 47 | 0.88 | 20 |
| 1 | 3.22 | 3.28 | 36 | 0.95 | 20 |
| 2 | 4.25 | 3.1 | 33 | 1.25 | 20 |
| 0 | 0.835 | Not-measured | 342 | Negligible | 50 |
| 1 | 0.888 | Not-measured | 318 | Negligible | 50 |
| 2 | 1.23 | Not-measured | 279 | Negligible | 50 |

is switched on, and Level 1 or Level 2 corresponds while $M_1$ or $M_2$ is switched on, respectively, while $M_0$ is on in 20 cm and 50 cm link ranges. The DC levels or SRs amounts depend on the $R_1$=56 Ω and $R_2$=6.8 Ω of circuit branches. Figure 10 demonstrates the variation of signals and measurements along with the input capacitor's charging time: the obtained input voltage, the SR and the average voltage of the detected signal, and the boost converter output voltage. The presented results correspond to two different input capacitor values (5 F and 9.4 mF) and three different DC levels in the transmitted signal over a transmission distance of 20 cm. The same metrics using a 9.4 mF input capacitor are also evaluated in a 50 cm link range and presented in Fig. 11. Due to the long charging time of the 5 F capacitor caused by the low average received power in the 50 cm link range due to high attenuation, the obtained results are not applicable for practical implementation. Therefore, to account for this in Tabs. 3, 4, the label (*Not-measured.*) is mentioned. As illustrated, the SR varies during the charging time of the input capacitor, reaching its maximum value when the capacitor is fully charged. The charging time ($t_{\mathrm{fc}}$) of the input capacitor for 5 F and 9.4 mF in different DC levels of the transmitted signal and LED illuminances are provided in Tab.3. Moreover, the maximum current ($I_{\mathrm{out}}$) that the boost converter can provide while keeping the output voltage constant at 3.3 V for 5 F and 9.4 mF in 20 cm link distance ($d$)

TABLE 4: Measured SNR and starting time of the boost converter.

| **Levels** | $SNR_{\mathrm{fc}}$ dB | $SNR_{\mathrm{s}}$ dB | $t_{\mathrm{s}}$**(9.4mF) (s)** | $t_{\mathrm{s}}$**(5F) (h)** | **d (cm)** |
|---|---|---|---|---|---|
| 0 | 56.2042 | 38.7320 | 10 | 0.692 | 20 |
| 1 | 49.4068 | 37.0615 | 9.5 | 0.583 | 20 |
| 2 | 38.8017 | 31.2986 | 7.5 | 0.475 | 20 |
| 0 | 54.4434 | 37.3867 | 57 | Not-measured | 50 |
| 1 | 47.6661 | 34.8507 | 54 | Not-measured | 50 |
| 2 | 36.9785 | 28.4218 | 42 | Not-measured | 50 |

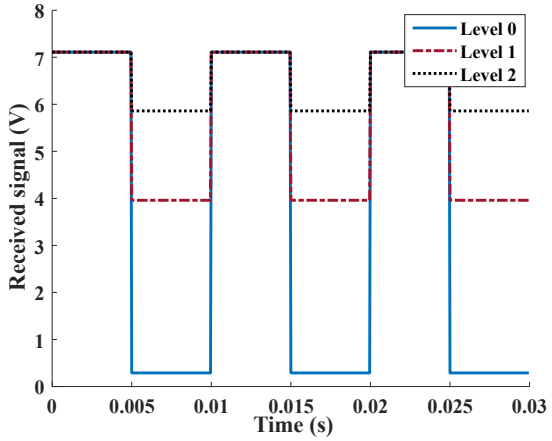


(a) d=20 cm link distance.

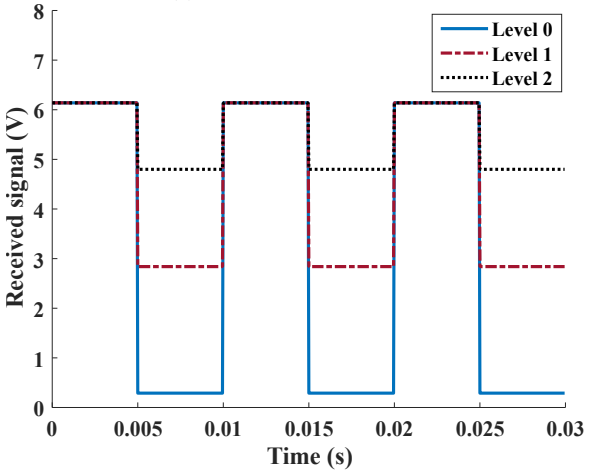


(b) d=50 cm link distance.

FIGURE 9: Received signal of the solar panel-based UWOC considering three different transmitted DC levels (a): in d=20 cm link distance, (b): in d=50 cm link distance.

is measured. However, the obtained current for the 50 cm link range is negligible to mention in the table and is displayed as a (*Negligible*) label. Table 4 demonstrates the system SNR over a transmission distance of 20 cm and 50 cm in two cases: once the input capacitor is fully charged ($SNR_{\mathrm{fc}}$) and once the boost converter starts working ($SNR_{\mathrm{s}}$). As shown, the obtained SNR in both starting the boost converter and when the input capacitor is fully charged is significantly promising. As depicted, the SNR decreases by increasing the DC level where the dominant effect for decreasing the SNR is reducing the SR, not increasing the noise due to the low variation of the standard deviation by increasing the transmitted power based on the solar cell I-V curve. The estimated BER for an NRZ-OOK modulation for each measured system SNR is given [23]:

$$BER_{\mathrm{NRZ-OOK}} = \frac{1}{2} erfc\left(\frac{1}{2\sqrt{2}}\left(\sqrt{SNR}\right)\right), \qquad (12)$$

where, erfc(x) is the complementary error function. According to (12), the maximum BER is lower than $10^{-10}$ for the obtained SNR of 28.42 dB, which is below the forward error correction (FEC) limit.

In addition, the boost converter starting time ($t_{\mathrm{s}}$) considering different signal DC levels for the 5 F and 9.4 mF capacitors values is shown. The results illustrate that the charging time of the input capacitor decreases with increasing the DC level. Moreover, the boost converter starting and capacitor charging times for the 5 F input capacitor in the 20 cm link span are reduced to 13 minutes and 30 minutes, respectively. Considering the 9.4 mF input capacitor with the highest DC level, the boost converter starting time and capacitor charging time are reduced to around 2.5 seconds, 15 seconds over the 20 cm link distance, and 12 seconds, 63 seconds for the 50 cm link distance, respectively. In all the cases, the system SNR is higher than 28 dB, and the BER is below the FEC limit; therefore, the signal can be detected and decoded when the boost converter starts working.

Note that the performance of the proposed transmission and reception circuits are primarily investigated and evaluated in simulation; however, due to the not actual model of the WLED and solar cell in the simulation, the results are not comparable with the experiment.

## V. CONCLUSION

In this work, a UWOC SLIPT system using a power splitting configuration was presented. This unidirectional system sends information while providing the necessary energy using the SLIPT paradigm to IoUT nodes. Unlike other approaches that separate power from a signal in a current-based scheme, this work focused on power splitting using the solar cell's voltage signal since the photovoltaic configuration was used. This configuration is sensitive to ambient light and other light sources that saturate the solar cell output and is

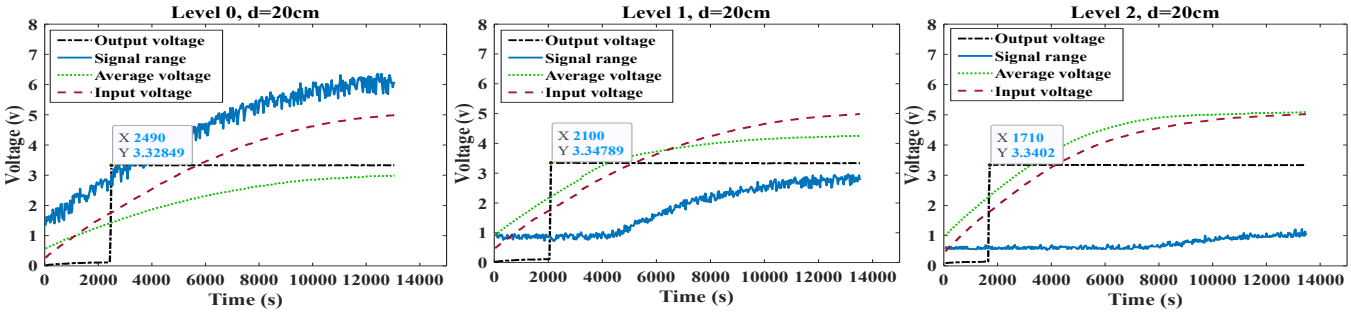


(a) Input capacitor=5 F, d=20 cm

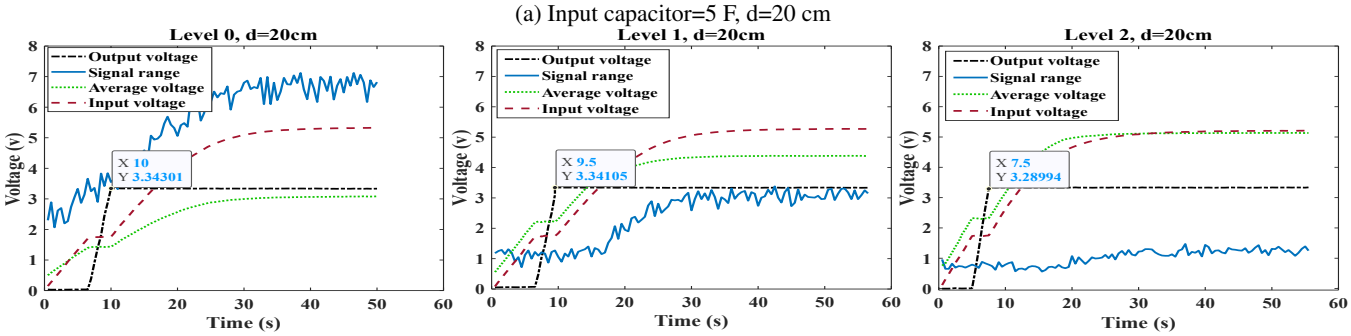


(b) Input capacitor=9.4 mF, d=20 cm

FIGURE 10: Experimental results demonstrating the output voltage of the boost converter, the averaged received signal, the amplitude of the signal and the input capacitor charging curve for 20 cm link ranges in three different DC levels for (**a**)5 F input capacitor, (**b**)9.4 mF input capacitor.

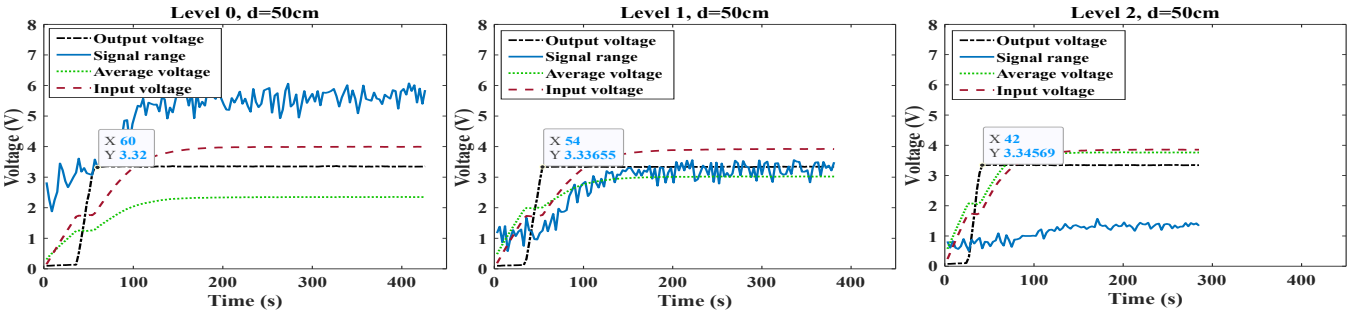


FIGURE 11: Experimental results demonstrating the output voltage of the boost converter, the averaged received signal, the amplitude of the signal and the input capacitor charging curve for 50 cm link ranges in three different DC levels for 9.4 mF input capacitor.

suitable for underwater scenarios where the background illumination is small enough to avoid undesired nonlinearities on the receiver. A novel transmission scheme was proposed with the capability of controlling the average transmitted power by adjusting the transmitted SRs or DC levels. This strategy could significantly improve the EH performance of a solar cell on the reception side, such as reducing the battery charging time and adapting the transmitted signal components to the different channel conditions or device state conditions. The received power was split into two branches for EH and ID. In this work, the receiver performance depended on the input capacitor voltage was considered in two stages. Then, the equations to model the receiver performance for each stage were expressed. The transmitter and receiver were simulated in LTspice to verify the performance of the proposed circuits. Simulation results illustrated that the proposed scheme could control the DC level; thus, the average transmitted power. Moreover, the underwater experimental setup based on the proposed system was presented. The obtained results under the laboratory testbed conditions showed the significant impacts of the DC level variation on the harvested energy rate. Furthermore, the evaluated system SNR with values higher than 28 dB and the BER of less than $10^{-10}$ which is below the FEC limit, showed that the data was detectable while the boost converter supplied the power of the IoUT nodes. Furthermore, the charging time of around 30 min and 15 seconds for 5 F and 9.4 mF, respectively, over a link span of 20 cm, and 63 seconds for 9.4 mF in 50 cm

link distance is improved. Therefore, the results confirm that the new proposed transmission scheme effectively decreases the EH capacitor recharging time, mainly for big ones (i.e., 5 F capacitor in this work). In addition, the link maintains adequate SNR and BER values that assure the data is received correctly.

## ACKNOWLEDGMENT

This work has been funded by the European Union's Horizon 2020 research and innovation programme under the Marie Skłodowska Curie grant agreement ENLIGHTEM No. 814215.

## REFERENCES

[1] M. F. Ali, D. N. K. Jayakody, Y. A. Chursin, S. Affes, and S. Dmitry, "Recent advances and future directions on underwater wireless communications," Archives of Computational Methods in Engineering, vol. 27, no. 5, pp. 1379–1412, 2020.

[2] M. Stojanovic and J. Preisig, "Underwater acoustic communication channels: Propagation models and statistical characterization," IEEE communications magazine, vol. 47, no. 1, pp. 84–89, 2009.

[3] X. Che, I. Wells, G. Dickers, P. Kear, and X. Gong, "Re-evaluation of rf electromagnetic communication in underwater sensor networks," IEEE Communications Magazine, vol. 48, no. 12, pp. 143–151, 2010.

[4] C. Pontbriand, N. Farr, J. Ware, J. Preisig, and H. Popenoe, "Diffuse high-bandwidth optical communications," in OCEANS 2008. IEEE, 2008, pp. 1–4.

[5] M.-A. Khalighi, C. Gabriel, T. Hamza, S. Bourennane, P. Leon, and V. Rigaud, "Underwater wireless optical communication; recent advances and remaining challenges," in 2014 16th International Conference on Transparent Optical Networks (ICTON). IEEE, 2014, pp. 1–4.

[6] G. Schirripa Spagnolo, L. Cozzella, and F. Leccese, "Underwater optical wireless communications: Overview," Sensors, vol. 20, no. 8, p. 2261, 2020.

[7] W. C. Cox Jr, Simulation, modeling, and design of underwater optical communication systems. North Carolina State University, 2012.

[8] L. Mullen, A. Laux, and B. Cochenour, "Propagation of modulated light in water: implications for imaging and communications systems," Applied optics, vol. 48, no. 14, pp. 2607–2612, 2009.

[9] P. D. Diamantoulakis, G. K. Karagiannidis, and Z. Ding, "Simultaneous lightwave information and power transfer (slipt)," IEEE Transactions on Green Communications and Networking, vol. 2, no. 3, pp. 764–773, 2018.

[10] G. Pan, P. D. Diamantoulakis, Z. Ma, Z. Ding, and G. K. Karagiannidis, "Simultaneous lightwave information and power transfer: Policies, techniques, and future directions," IEEE Access, vol. 7, pp. 28 250–28 257, 2019.

[11] M. Uysal, S. Ghasvarianjahromi, M. Karbalayghareh, P. D. Diamantoulakis, G. K. Karagiannidis, and S. M. Sait, "Slipt for underwater visible light communications: Performance analysis and optimization," IEEE Transactions on Wireless Communications, 2021.

[12] M. Kong, C. H. Kang, O. Alkhazragi, X. Sun, Y. Guo, M. Sait, J. A. Holguin-Lerma, T. K. Ng, and B. S. Ooi, "Survey of energy-autonomous solar cell receivers for satellite–air–ground–ocean optical wireless communication," Progress in Quantum Electronics, p. 100300, 2020.

[13] C. Gabriel, M.-A. Khalighi, S. Bourennane, P. Léon, and V. Rigaud, "Misalignment considerations in point-to-point underwater wireless optical links," in 2013 MTS/IEEE OCEANS-Bergen. IEEE, 2013, pp. 1–5.

[14] M. Kong, B. Sun, R. Sarwar, J. Shen, Y. Chen, F. Qu, J. Han, J. Chen, H. Qin, and J. Xu, "Underwater wireless optical communication using a lens-free solar panel receiver," Optics Communications, vol. 426, pp. 94–98, 2018.

[15] W. Liu, Z. Xu, and L. Yang, "Simo detection schemes for underwater optical wireless communication under turbulence," Photonics Research, vol. 3, no. 3, pp. 48–53, 2015.

[16] X. Chen, W. Lyu, C. Yu, Y. Qiu, Y. Shao, C. Zhang, M. Zhao, J. Xu, and L.-K. Chen, "Diversity-reception uwoc system using solar panel array and maximum ratio combining," Optics express, vol. 27, no. 23, pp. 34 284–34 297, 2019.

[17] M. Kong, J. Lin, C. H. Kang, C. Shen, Y. Guo, X. Sun, M. Sait, Y. Weng, H. Zhang, T. K. Ng et al., "Toward self-powered and reliable visible light communication using amorphous silicon thin-film solar cells," Optics express, vol. 27, no. 24, pp. 34 542–34 551, 2019.

[18] M. Kong, J. Lin, Y. Guo, X. Sun, M. Sait, O. Alkhazragi, C. H. Kang, J. A. Holguin-Lerma, M. Kheireddine, M. Ouhssain et al., "Aquae-lite hybrid-solar-cell receiver-modality for energy-autonomous terrestrial and underwater internet-of-things," IEEE Photonics Journal, vol. 12, no. 4, pp. 1–13, 2020.

[19] J. I. de Oliveira Filho, A. Trichili, B. S. Ooi, M.-S. Alouini, and K. N. Salama, "Toward self-powered internet of underwater things devices," IEEE Communications Magazine, vol. 58, no. 1, pp. 68–73, 2020.

[20] S. Zhang, D. Tsonev, S. Videv, S. Ghosh, G. A. Turnbull, I. D. Samuel, and H. Haas, "Organic solar cells as high-speed data detectors for visible light communication," Optica, vol. 2, no. 7, pp. 607–610, 2015.

[21] C. T. Geldard, J. Thompson, and W. O. Popoola, "Empirical study of the underwater turbulence effect on non-coherent light," IEEE Photonics Technology Letters, vol. 32, no. 20, pp. 1307–1310, 2020.

[22] D. Menaka and S. Gauni, "Ocean of things: Marine environment monitoring using discriminatory model," in Journal of Physics: Conference Series, vol. 1964, no. 7. IOP Publishing, 2021, p. 072015.

[23] T. Y. Elganimi, "Studying the ber performance, power-and bandwidth-efficiency for fso communication systems under various modulation schemes," in 2013 IEEE Jordan Conference on Applied Electrical Engineering and Computing Technologies (AEECT). IEEE, 2013, pp. 1–6.

BEHNAZ MAJLESEIN received her B.Sc. and M.Sc degrees in electrical engineering from the Isfahan University of Technology, Iran, in 2015 and 2019. She is currently pursuing a Ph.D. at the Universidad de Las Palmas de Gran Canaria, Spain while working as an early stage researcher of Marie Cuire ENLIGHTEM project for the LightBee company. Her research interest includes energy-efficient underwater wireless optical communications.

VICTOR GUERRA received a doctorate award in the engineering and architecture branch (ULPGC, 2018). He is a former researcher at the photonics and communications division of the IDeTIC university institute since 2008 and he is currently Senior Researcher at Pi Lighting, Switzerland. He has participated in 5 H2020 projects, 4 national projects, 2 regional projects, and several contracts with highly relevant private companies. He has published over 50 articles in indexed journals and conference papers. His current research interests are wireless optical communications (atmospheric and underwater), optical camera communications, and artificial intelligence applications.

JOSE RABADAN received the M.S. in 1995 and his PhD. in 2000, both at the University of Las Palmas de Gran Canaria. He is currently a full professor and researcher attached to the IDeTIC University Institute. His research interests are in the field of wireless optical communications, visible light communication systems, and optical communications with cameras, where he works on high-performance coding and modulation schemes and channel estimation techniques. He has been a researcher in different national and international projects financed by national and European administrations and companies. He is also the author of 3 book chapters, more than 30 articles in international journals, and more than 90 conference papers.

JULIO RUFO received his M.S. and PhD., both at the University of Las Palmas de Gran Canaria. He obtained, in 2022, a Ramon y Cajal grant from the Spanish Ministry of Science, and he has joined Universidad de La Laguna as a researcher while he is the CTO of LightBee. His research interests are in the field of wireless optical communications working on architecture, protocols, and applications for sensor networks and IoT technologies.

RAFAEL PEREZ-JIMENEZ was born in Madrid in 1965. Eng and MSc (1991) Ph.D. in Telecommunications engineering (1995, Honors) and History (2020, Honors), Full Professor at the School of Telecommunication Engineering of the ULPGC (University of Las Palmas de Gran Canaria) from 2003, and Chairman of the photonics division of IDeTIC (University Institute for Technological Development and Innovation in communications) since its foundation (2010). He has participated in or directed 11 transnational projects (2 runnings), 26 official national projects in competitive calls, and a score of relevant contracts with companies and administrations. He has published 4 teaching books, 5 book chapters, and over 250 peer-reviewed papers in journals and international technical conferences. He is a frequent reviewer in different international magazines and symposia (within the IEEE, IET, OSA, MDPI, and others) as well as an evaluator in different research national agencies. Its main area of specialization corresponds to developing wireless optical communication systems, especially for IoT sensor networks and medium/low-speed links, including both the vehicular and domestic environment, and the characterization of optical channels in indoor and mobile systems. He is also working on applications of optical wireless communications and the internet of things over Smart Cities.